ELEMENTA
Science of the Anthropocene

López-García, V, et al. 2022. Low-level jets over the Arctic Ocean during MOSAiC. *Elem Sci Anth*, 10: 1. DOI: https://doi.org/10.1525/elementa.2022.00063

RESEARCH ARTICLE

# Low-level jets over the Arctic Ocean during MOSAiC

Vania López-García[1,*], Ryan R. Neely III[1,2], Sandro Dahlke[3], and Ian M. Brooks[1,*]

We present an annual characterization of low-level jets (LLJs) over the Arctic Ocean using wind profiles from radiosondes launched during the Multidisciplinary drifting Observatory for the Study of Arctic Climate expedition, from October 2019 through September 2020. Our results show LLJs to be common throughout the entire year, with a mean annual frequency of occurrence of more than 40%, a typical height below 400 m, peaking at 120–180 m, and speed between 6 and 14 m $s^{-1}$. Jet characteristics show some seasonal variability: During winter and the freeze-up period, they are more common and faster, with an average occurrence of 55% and speeds of 8–16 m $s^{-1}$, while in summer and the transition period, they have a mean occurrence of 46% and speeds of 6–10 m $s^{-1}$. They have a similar height all year, with a peak between 120 and 180 m. The ERA5 reanalysis shows a similar frequency of occurrence, but a 75 m high bias in altitude, and a small, 0.28 m $s^{-1}$, slow bias in speed. The height biases are greater in the transition period, more than 130 m, while the bias in speed is similar all year. Examining jets in ERA5 over the full year and whole Arctic Ocean, we find that the frequency of occurrence depends strongly on both the season and the distance to the sea-ice edge.

**Keywords:** Low-level jet, Arctic Ocean, MOSAiC, Annual cycle, Frequency of occurrence

## 1. Introduction

The Arctic is warming at more than twice the average global rate (Serreze et al., 2009; Overland et al., 2019), a phenomenon commonly called Arctic amplification. Even after decades of research, climate models, although improving, still struggle to reproduce correctly the observed rate of change of the Arctic climate system. There is also much greater scatter between different models in the Arctic than at lower latitudes (Holland and Bitz, 2003). One area of model weakness is the representation of the vertical structure of the atmospheric boundary layer in the Arctic (Brooks et al., 2017; Tjernström et al., 2021); even reanalyses poorly represent temperature inversions here (Graham et al., 2019). Over sea ice, in summer, the Arctic boundary layer typically has near-neutral stability, while in winter, it is often stable. In neutral and stable boundary layers, turbulence is mainly generated by vertical shear of the horizontal wind (Banta et al., 2003), and in the presence of cloud, by radiative cooling at cloud top (Shupe et al., 2013). Low-level jets (LLJs) are a potentially important additional source of turbulent mixing for both the cloud-capped and cloud-free Arctic boundary layer, providing a source of turbulence from above that models typically fail to reproduce accurately, affecting their representation of mixing in the boundary layer.

An LLJ is a local maximum in the vertical profile of the horizontal wind speed, typically found below 2,000 m (Bonner, 1968; Andreas et al., 2000; Tuononen et al., 2015). LLJs have been broadly studied worldwide due to their relevance to regional weather—they can influence the horizontal transport of gases, aerosols, and moisture, which can consequently modify precipitation patterns. LLJs with strong vertical wind shear can generate turbulence aloft and impact the turbulent exchange between the surface and the atmosphere (Conangla and Cuxart, 2006) and hence influence the surface energy budget. This may be a significant source of heat to the surface if the jet is associated with a strong, low-level inversion, such as during warm air intrusions (Tjernström et al., 2015; Tjernström et al., 2019).

Global models struggle to represent properly the Arctic boundary layer (Birch et al., 2012; Sotiropoulou et al., 2016; Graham et al., 2019; Tjernström et al., 2021; Young et al., 2021). They may have an inadequate vertical resolution, particularly around the inversion at the boundary layer top and poorly represent many physical processes relevant to boundary-layer dynamics. Graham et al. (2019) showed that the newest product of the European Centre for Medium-Range Weather Forecasts (ECMWF), ERA5, improved greatly its representation of LLJ strength in comparison with their former product, ERA-Interim, in an Arctic gateway during summer. However, Kalverla et al. (2019), using data for 10 years over the Dutch North Sea, concluded that ERA5, although capturing correctly the LLJ seasonal cycle, still

[1] School of Earth and Environment, University of Leeds, Leeds, UK
[2] National Centre for Atmospheric Science, University of Leeds, Leeds, UK
[3] Alfred Wegener Institute, Helmholtz Centre for Polar and Marine Research, Bremerhaven, Germany

* Corresponding authors:
Emails: eevnlg@leeds.ac.uk; i.m.brooks@leeds.ac.uk

has biases in the speed and height of LLJs when compared to observations.

Although LLJs are well-studied features at low latitudes, there are fewer studies in the Arctic, and their frequency of occurrence, properties, and generation mechanisms here are not well characterized. Studies have suggested that the most common forcing mechanisms are baroclinity (Guest et al., 2018), inertial oscillations (Jakobson et al., 2013), and katabatic flows in coastal regions (Tuononen et al., 2015). Moreover, Guest et al. (2018), related LLJ forcing mechanisms to their basic characteristics, finding that LLJs due to baroclinity are the shallower and last longer, while LLJs due to inertial oscillations are faster but can disappear quickly.

There is little consensus on the frequency and seasonal variability of LLJs in the Arctic. Jakobson et al. (2013) made tethered balloon soundings during the drift of the Tara across the central Arctic Ocean from late April through August 2007 and found an LLJ occurrence of approximately 50%. Tjernström et al. (2004) used radiosonde soundings during the drift of Oden over the central Arctic Ocean for almost all of August 2001 and found a frequency of occurrence around 25%. Under the assumption that LLJs are more common during the colder season, Tuononen et al. (2015) assembled an 11-year climatology of LLJs from the Arctic System Reanalysis (ASR-Interim; Bromwich et al., 2010; Bromwich et al., 2015) to study jet properties during late autumn and winter (October–March). They found an occurrence of 20%–25% for the central Arctic and around 50%–60% close to the sea-ice edge in March; typical jet heights were below 350 m and speeds around 8–12 m $s^{-1}$. Ranjha et al. (2013) analyzed the seasonal variability of coastal LLJs using ERA-Interim reanalysis from 1980 to 2011. They argued that the sea-ice edge can be treated as a dynamic coastline and found a frequency of occurrence of about 30% from December to February, but less than 15% from June to August.

Although these previous observational studies have expanded our understanding of LLJs in the Arctic, they provide a very sparse data set and lack either interseasonal data or wide geographical coverage since none of them covers all the different seasons and the majority were conducted close to the marginal ice zone. Therefore, a better characterization of the basic characteristics and seasonal variability of LLJs is needed.

Here, we characterize LLJs over the Arctic pack ice for a full year using measurements from the radiosonde program during the Multidisciplinary drifting Observatory for the Study of Arctic Climate (MOSAiC) expedition (Shupe et al., 2022). We use our results to evaluate the representation of LLJs in ERA5, while also using ERA5 to put the observations along the ship's drift track into the wider spatial context of the whole Arctic Ocean.

## 2. Data and methods

MOSAiC aimed to make measurements of all components of the Arctic climate system over a full calendar year (Nicolaus et al., 2022; Rabe et al., 2022; Shupe et al., 2022). It was based on the icebreaker Polarstern (Knust, 2017). The MOSAiC cruise lasted from late September

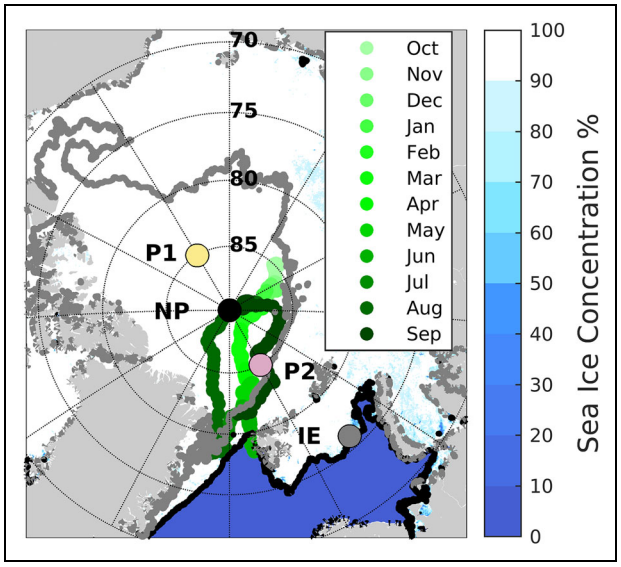


**Figure 1. The cruise track of the Polarstern during the Multidisciplinary drifting Observatory for the Study of Arctic Climate expedition**. Path of Polarstern from October 2019 to September 2020. Sea-ice concentration is shown for March 5, 2020, which corresponds to the day of maximum sea-ice extent of 2020 (NSIDC.org). The black line shows the sea-ice edge (sea-ice concentration at least 15%) for the day of maximum sea-ice extent, and the gray line for the minimum (September 15, 2020). For future reference, points are marked at the North Pole (NP); P1 and P2 have the same latitude but opposite longitude, −150° and 30°, respectively; and one point at the ice edge (IE), moving with latitude but constant longitude of 45° following the sea-ice edge.

2019 to early October 2020, with Polarstern frozen into the sea ice, during most of the duration of the campaign, from October 4 to September 20 (**Figure 1**). An overview of all the atmospheric science measurements is given in Shupe et al. (2022). During MOSAiC, radiosondes (Väisälä RS41-SGP) were launched every 6 h (0000, 0600, 1200, and 1800 UTC) and occasionally more frequently during some significant weather events, such as storms systems. Here, for consistency, we do not use the extra launches but data from the routine launches only from October 1, 2019 to September 30, 2020. The radiosondes provide vertical profiles of wind speed and direction, temperature, relative humidity, and pressure with a vertical resolution of approximately 5 m, from 12 m—the altitude of the helideck from which they were launched—up to a maximum altitude of about 30 km. We only use data from above 50 m, since measurements in the lowest few tens of meters above the ship can be influenced by the ship (Achtert et al., 2015). There were two breaks in the wider measurement program: May 16–June 19, when the ship had to transit to Svalbard to exchange crew and the science team, and July 31–August 21, when the original ice floe broke up near the ice edge and the Polarstern repositioned back into the central Arctic. Neither of these breaks significantly affected the radiosonde measurements,

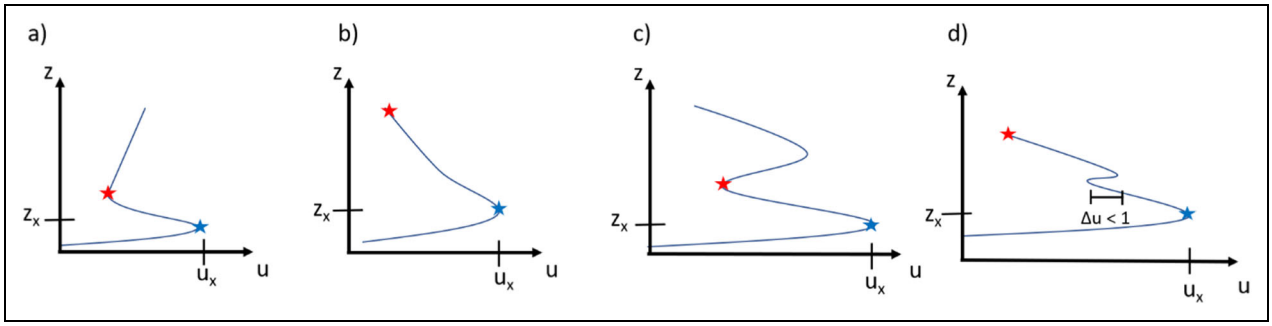


**Figure 2. Sketch diagrams of wind speed profiles and the identification of low-level jets (LLJs).** The blue star is the wind speed maximum classified as an LLJ, while the red star is the first minimum in wind speed above the jet. (a) A typical LLJ. (b) In case of no minimum, the wind speed at the highest altitude is used. (c) In case of two jets, the LLJ is taken to be the one at lowest altitude. (d) Any local minimum less than 1 m $s^{-1}$ is ignored. $u_x$ and $z_x$ are the LLJ speed and height, respectively. Adapted from Tuononen et al. (2015).

which were launched from the ship and continued throughout transits, except for a gap from June 3 to 8, when the ship was in territorial waters around Svalbard.

Each radiosonde provides measurements at a single location and time; the drift of the ship with the ice means that spatial and seasonal variability are difficult to separate. In order to put the measurements into a wider geographical and temporal context, we utilize data from the fifth generation of the ECMWF atmospheric reanalysis of the global climate (ERA5; Hersbach et al., 2020). ERA5 is the highest resolution global reanalysis product to date, with an approximately 31 km horizontal grid, 137 pressure levels up to 80 km, and 1 h temporal resolution.

For the purpose of this study, for both the observations and ERA5, we analyzed the vertical profile of the horizontal wind speed over the lowest 4 km. To assess the performance of ERA5 in reproducing the observed LLJs, we used the closest model grid point to Polarstern's location and the closest time to the actual launch times (typically about 45 min before the synoptic hour). We disregard the distance from the closest grid point to the ship's location (less than 15 km), the time difference between ERA5 output and the launch time of the radiosonde (typically less than 15 min), the time the balloon takes to rise up to the maximum height used (less than 5 min), and the horizontal distance that the radiosonde may travel while ascending.

Finally, to provide a wider geographical context to the results along the ship track, we search for LLJs across the entire Arctic Ocean from October 2019 to September 2020 in the ERA5 data using a grid of 0.25° × 0.25° and the lowest 37 model levels (the lowest 4,000 m).

### *2.1. Criteria for LLJ detection*

The precise criteria used to identify an LLJ vary between studies according to their objectives (Bonner, 1968; Banta et al., 2002; Jakobson et al., 2013). Here, we use a definition based on the most common one in the literature (Bonner, 1968; Andreas et al., 2000; Tuononen et al., 2015). An LLJ is defined as a local maximum in the vertical profile of wind speed of at least 2 m $s^{-1}$ and 25% higher than the minimum above it and located below 1500 m, as illustrated in **Figure 2a**. In the case of a maximum with no well-defined minimum above, the wind speed at the top of the profile is used as the minimum (**Figure 2b**). In the case where two or more jets are found below 1,500 m, we only analyze the lowest one (**Figure 2c**). Finally, any local maxima or minima less than 1 m $s^{-1}$, above or below the primary maximum, is ignored (**Figure 2d**). Tuononen et al. (2015) restricted the upper limit of the wind speed profile to 1,500 m; however, we find that while increasing this upper limit makes little difference to the identification of jets from the radiosonde data, it has a significant impact on the number found in ERA5. For this reason, we increase the upper limit of altitude searched for the wind speed minimum above the jet to 4,000 m (see description Text S1 and Figures S1–S3 for details).

## 3. Results

### *3.1. Observations*

**Figure 3** shows the time series for LLJ height and speed for both observations and ERA5 profile for the full duration of MOSAiC, along with the surface wind speed, pressure, and air temperature. The seasons are indicated following Shupe et al. (2022). See Figure S4 for expanded figures that more clearly show the details in the times series.

The occurrence of jets in the observations is relatively uniform throughout the year and broadly reproduced in ERA5. The frequency of occurrence is shown by month in **Figure 4**; it varies from 42% to 62% with an annual mean of 51%. The frequency is greatest in October and November, with LLJs occurring at least 60% of the time. The variation through the remainder of the year is limited, with no clear seasonal cycle. To investigate this further, we average the occurrence by season (autumn freeze-up: September 6 to November 25, winter: November 26 to April 14, transition: April 15 to May 26, and summer melt: May 27 to September 5), finding jets 62%, 47%, 43%, and 49% of the time, respectively.

The speed of the jets (**Figure 3**) clearly reflects that of the near-surface wind with the highest values associated with low pressure systems. Variations in surface pressure,

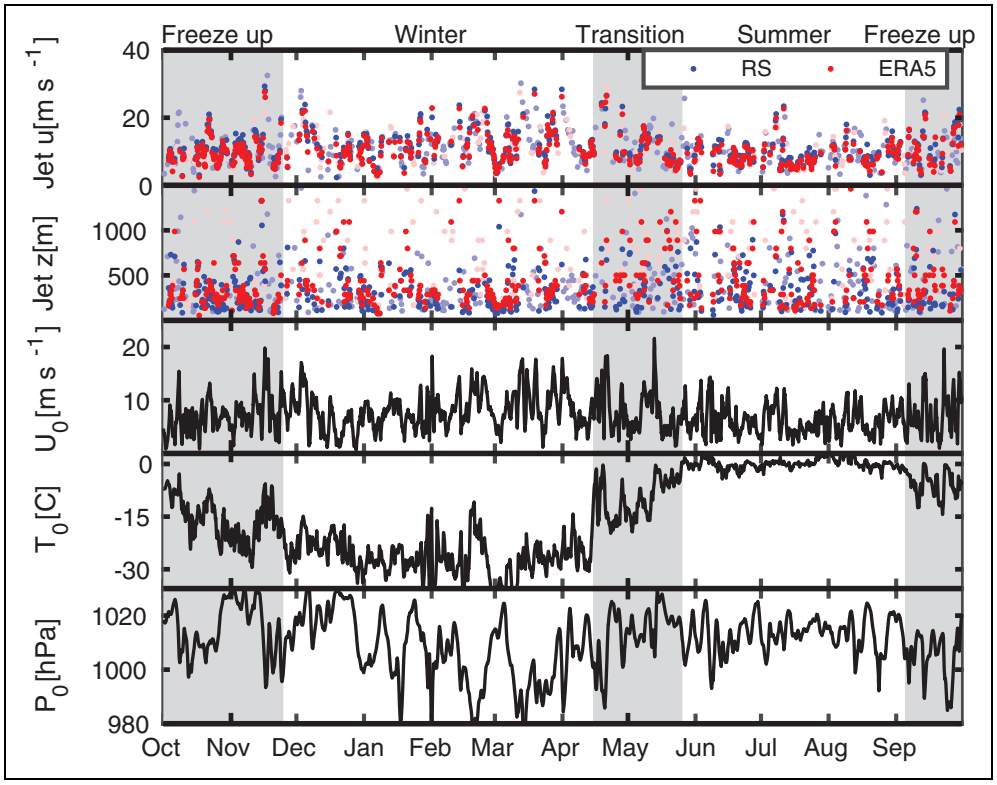


**Figure 3. Time series of the low-level jet (LLJ) height and speed**. Speed and height of all LLJs found for each data set from October 2019 to September 2020. Shaded areas separate the seasons following Shupe et al. (2022). Blue and red markers show jets from the observations and ERA5, respectively. Dark shades indicate a jet occurs in both the observations and ERA5, and pale shades indicate that a jet was found only in the observations or ERA5, but not both. Surface pressure, wind speed, and air temperature are from the Polarstern's on-board meteorological measurements.

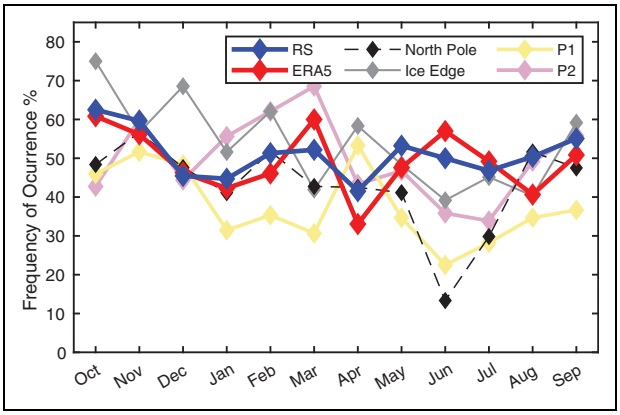


**Figure 4. Frequency of occurrence of low-level jets (LLJs) in the Arctic for an annual cycle LLJ**. Comparison of the frequency of occurrence of LLJs per month from October 2019 to September 2020, from the radiosonde program within Multidisciplinary drifting Observatory for the Study of Arctic Climate expedition (blue), the ERA5 model grid closest to Polarstern (red), and the four points marked in **Figure 1** (the same pale colors).

and hence wind speed, are greater in winter than summer; this is reflected in tighter clustering of the jet speed in summer. Conversely, the jet heights appear more tightly clustered during winter. Probability distributions of observed jet speed and height, for the full year and partitioned by season, are shown in **Figure 5**. The peak in the overall distribution of jet height is at 120–180 m, with a steep drop off for lower altitudes and a long tail for higher altitudes; very few jets are observed about 1,000 m. The peak is reasonably consistent throughout the year, with a slight tendency for LLJs to be lower during winter and the freeze-up period: 79% of the total number of LLJs for these seasons were below 400 m, while only around 60% were during the transition period and summer. LLJ speed shows a more distinct variation between seasons. It varies between 4 and 24 m $s^{-1}$ with a distinct peak at 8–10 m $s^{-1}$ (**Figure 5**) over the full year. The same peak value is seen in summer and the freeze-up period. During winter, the peak is shifted to higher speeds, of 12–14 m $s^{-1}$, consistent with generally higher winds over this period, while in the transition period, it is slightly lower, at 6–8 m $s^{-1}$, although the short duration of the transition period means there are few jets, and the statistics are less robust.

**Table 1** shows the LLJ speed and height statistics for the entire radiosonde and ERA5 data sets. ERA5 has a constant bias in LLJ speed median of less than –1 m $s^{-1}$ for all the seasons. While ERA5 bias in LLJ height changes between seasons, being minimum at the freeze-up period, difference in the median of 50 m, and maximum in the transition period and summer, being close to 300 and 120 m, respectively.

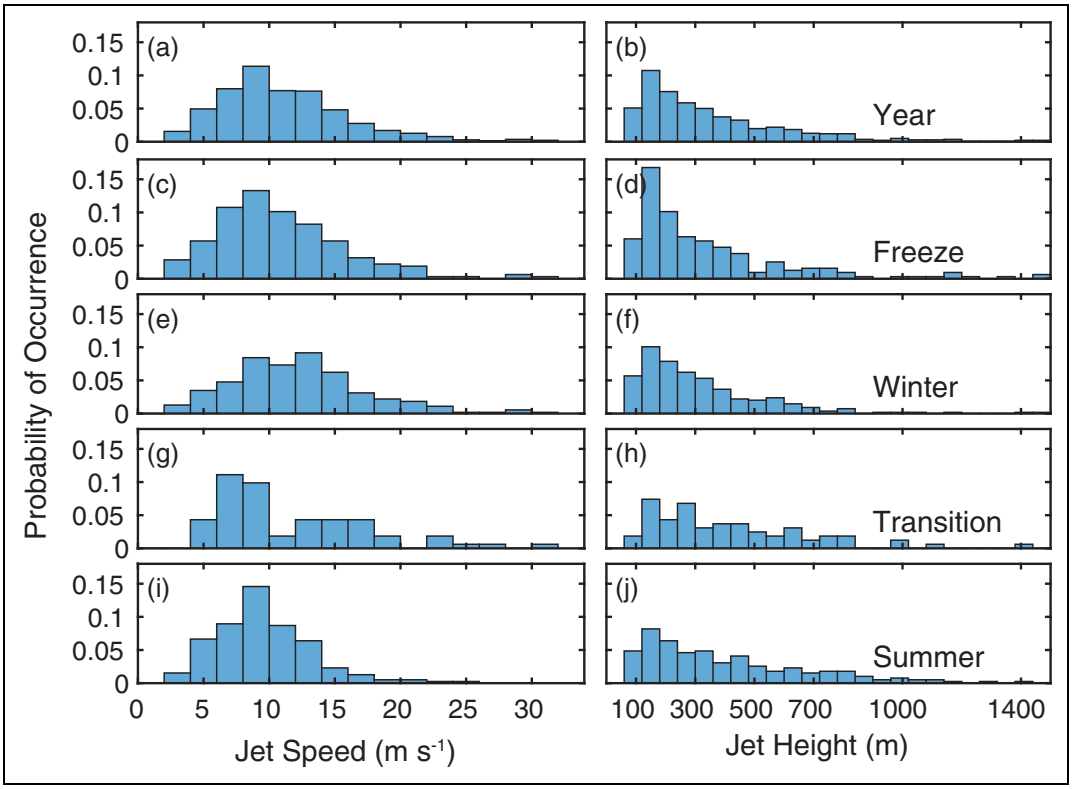


**Figure 5. Probability distributions for low-level jet (LLJ) height and speed per season for observations**. Comparison of probability distributions for LLJ speed (a, c, e, g, i) and height (b, d, f, h, j) for the full year (a, b) and divided by season: freeze-up (c, d), winter (e, f), transition (g, h), and summer (i, j). Bin widths are 2 m $s^{-1}$ for speed and 60 m for jet height.

**Table 1. The median, 25th and 75th percentiles of low-level jet (LLJ) speed (m $s^{-1}$) and height (m) for both radiosondes (RSs) and ERA5 for the entire data sets**

| | | No. of LLJs | | LLJ Speed (Median) | | LLJ Speed (25th Percentile) | | LLJ Speed (75th Percentile) | | LLJ Height (Median) | | LLJ Height (25th Percentile) | | LLJ Height (75th Percentile) | |
|---|---|---|---|---|---|---|---|---|---|---|---|---|---|---|---|
| **Season** | **No. of Profiles** | **RS** | **ERA5** | **RS** | **ERA5** | **RS** | **ERA5** | **RS** | **ERA5** | **RS** | **ERA5** | **RS** | **ERA5** | **RS** | **ERA5** |
| Full year | 1,415 | 758 | 693 | 10.1 | 9.6 | 7.7 | 7.2 | 13.5 | 13.0 | 275 | 385 | 160 | 245 | 450 | 638 |
| Freeze-up | 316 | 208 | 182 | 10.0 | 9.5 | 7.7 | 7.2 | 13.6 | 12.0 | 237 | 287 | 158 | 245 | 410 | 501 |
| Winter | 546 | 273 | 255 | 11.8 | 11.2 | 8.6 | 8.4 | 15.0 | 14.7 | 245 | 334 | 155 | 245 | 390 | 567 |
| Transition | 162 | 74 | 72 | 9.6 | 9.3 | 7.4 | 7.2 | 15.1 | 14.1 | 350 | 638 | 210 | 441 | 580 | 889 |
| Summer | 391 | 203 | 184 | 9.0 | 8.1 | 7.2 | 6.1 | 11.6 | 11.0 | 320 | 440 | 176 | 245 | 544 | 798 |

**Figure 6** shows the angle of rotation in the wind direction between the surface and jet peak (**Figure 6a**) and jet peak and jet top (defined as the height of the wind speed minimum above the peak, following the LLJ criteria used in Section 2.1; **Figure 6b**). For the majority of cases, the turning angle is positive (clockwise) with increasing altitude between the surface and jet peak, consistent with an Ekman spiral and inertial forcing (Andreas et al., 2000). The distribution of turning angles between the peak of the jet and minimum wind speed above is close to zero, implying the wind direction remained almost constant above the jet peak; this is consistent with baroclinic forcing (Guest et al., 2018). A detailed examination of the forcing processes for the jets is beyond the scope of this study but will be the subject of a future paper.

#### 3.2.1. Evaluation of ERA5 against observations

ERA5 does an efficient job of reproducing the number of LLJs throughout the entire year (**Figures 3** and **4**). However, there are some periods with inconsistencies in the frequency of occurrence between ERA5 and the observations. For example, in early April and early February, the radiosondes captured several LLJs, but ERA5 fails to reproduce the majority of them. In contrast, there are other

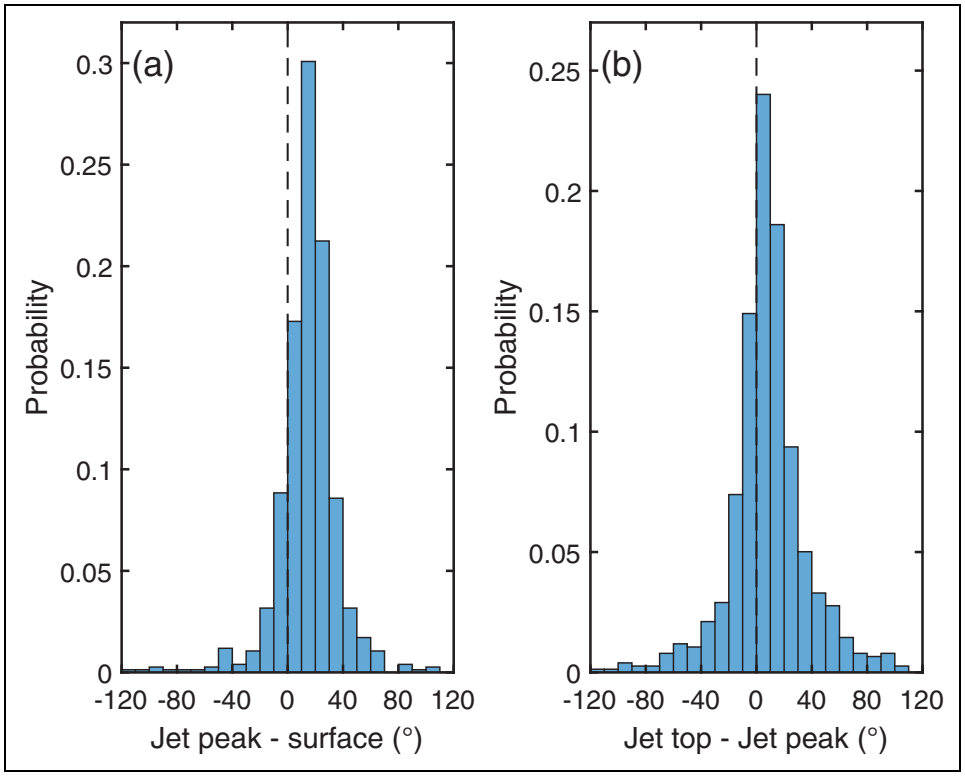


**Figure 6. Wind direction turning angles**. Probability distributions of the angles of rotation in the wind direction between (a) the surface and jet height and (b) the jet peak and top. Differences are defined as upper–lower level. Jet top is defined as the altitude of the wind-speed minimum above the jet peak according to the low-level jet criteria in **Figure 2**. Positive rotations are clockwise moving upwards. There are 12 cases with a turning angles greater than 120° (not shown). Bin widths are 10°.

periods, such as mid-October to mid-November, late December, and late-February, when ERA5 reproduces not only the presence of LLJs but also their speed and height.

In **Figure 7**, we compare the probability distributions of jet properties for the observations and ERA5. In order to conduct a like-for-like comparison, we consider only cases where LLJs were found within both the observational data and ERA5 (the LLJs in this subset are represented as dark points in **Figure 3**). ERA5 uses a vertical grid with intervals that increase with height. For convenience, we evaluate the ERA5 jet height statistics on model levels, and the observed jets in altitude bins centered on the model levels, with boundaries halfway between levels. The counts in each bin are then normalized by bin width and the total number of jets in each season, to give relative probabilities per unit altitude.

ERA5 tends to have LLJs at higher altitudes than observed throughout the year, with a peak in the distribution at around 280 m compared with 150 m for the observations. However, there is a seasonal difference in its performance. The peak in the distributions of observed LLJ height is always below 250 m, lowest in winter, the freeze-up and the transition period (150 m), and highest in summer (215 m). In contrast, the peak in ERA5 distributions is always at or above 240 m and is highest during the winter and the transition period (280 and 500 m, respectively) and lowest in the freeze-up and summer (244 and 287 m, respectively), when the overall distribution most closely matches that of the observed jets, although the peak jet height remains slightly higher than that for the observations.

In contrast to the jet height, ERA5 captures the jet speeds well, with only a small mean bias of about –0.6 m $s^{-1}$ throughout the year. Winter has the smallest bias of –0.4 m $s^{-1}$, while it is greater in summer, with a bias of –0.8 m $s^{-1}$.

**Table 2** summarizes the median biases (ERA5-observations) in the LLJ characteristics for the same vertical profiles. The median error in LLJ height is the lowest during summer, at about 55 m higher, and increases in the colder months reaching a maximum during the transition period, at just over 145 m higher. For the speed, the seasonal variation in bias is the opposite: Summer has the greatest LLJ speed mean error, 0.80 m $s^{-1}$ slower, which decreases in the colder months and reaches a minimum in the winter, 0.37 m $s^{-1}$ slower.

The relationship between the model and radiosonde values of speed and height for all the jets occurring in both is examined in more detail in **Figure 8**. The ERA5 LLJ speeds cluster tightly about the observed speeds (**Figure 8a**), with a small low bias that increases linearly with the jet speed. The ERA5 LLJ heights are widely scattered about the observed values (**Figure 8b**). The handful of observed LLJs above 1,000 m is well captured by ERA5, but, in general, it overestimates LLJ height, increasingly so as the observed jets become shallower. This is clear seen in **Figure 8c**, where the ratio of jet heights from ERA5 and radiosonde, $Z_{ERA5}/Z_{RS}$, is shown as a function of $Z_{RS}$.

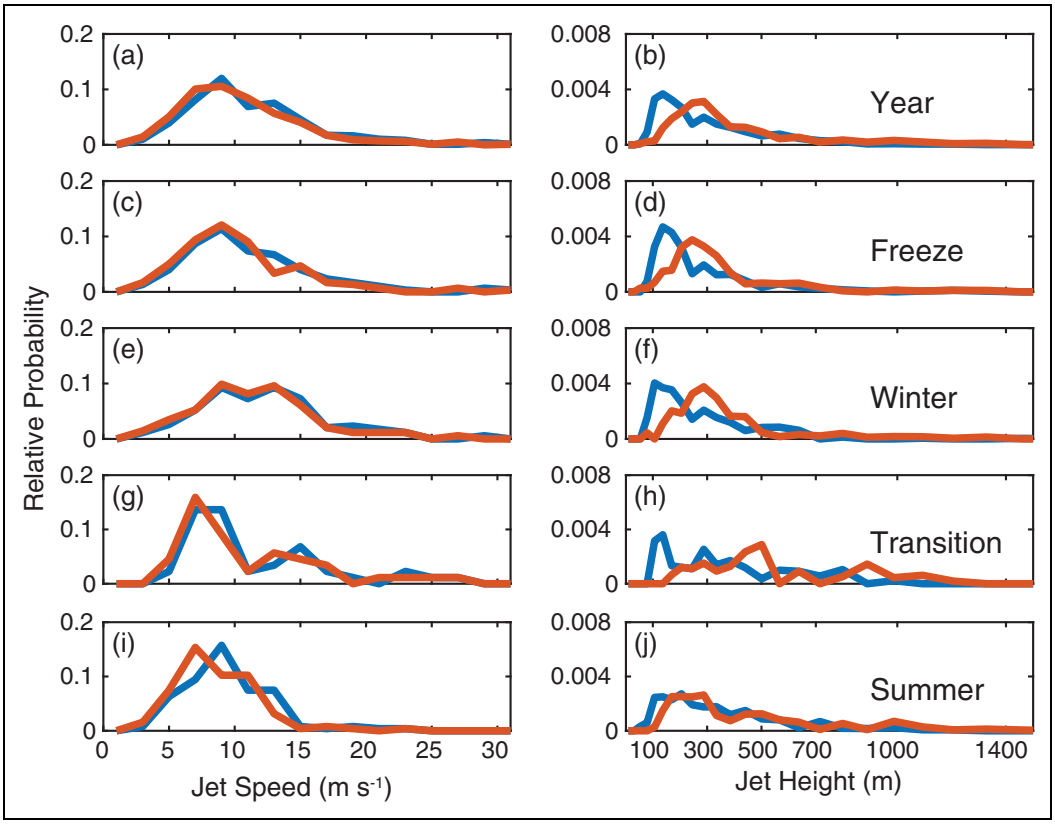


**Figure 7. Probability distributions of low-level jet (LLJ) height and speed per season for both observations and model**. Comparison of LLJ speed (a, c, e, g, i) and height (b, d, f, h, j) for LLJs that were found within both the radiosonde and ERA5, divided by seasons: all year (a, b), freeze-up (c, d), winter (e, f), transition (g, h), and summer (i, j). Probabilities are normalized by both bin width and total number of cases per season to give relative probability (0–1) per unit speed and altitude, respectively.

**Table 2. Median values in the properties of observed and model low-level jets (LLJs) and their differences (ERA5-observations) for the same vertical profiles**

| Properties | Freeze-up | Winter | Transition | Summer |
|---|---|---|---|---|
| No. of common LLJs | 145 | 166 | 42 | 123 |
| No. of total profiles | 316 | 546 | 162 | 391 |
| Observed height (m) | 210.0 | 225.0 | 327.5 | 310.0 |
| Modeled height (m) | 287.5 | 310.9 | 501.0 | 334.2 |
| Difference in height (m) | 77.5 | 87.5 | 145.1 | 54.7 |
| Observed Speed (m) | 9.8 | 11.7 | 9.1 | 8.8 |
| Modeled speed (m $s^{-1}$) | 9.2 | 11.0 | 8.9 | 8.1 |
| Difference in speed (m $s^{-1}$) | –0.6 | –0.4 | –0.7 | –0.8 |

A power law of the form $Z_{ERA5}/Z_{RS} = 29Z_{RS}^{-0.53}$ provides a good representation over most of the data range.

### 3.2.2. Pan-Arctic behavior in ERA5

To place the along-track results in a wider geographical context and separate the effects of temporal and spatial variability, **Figure 9** shows the frequency of occurrence of LLJs for the entire Arctic Ocean by month from ERA5. Tuononen et al. (2015) found that the highest occurrence is close to the sea-ice edge during the winter months. Here, we also find that the highest frequency of LLJs is during the colder months and close to the sea-ice edge. However, we also see that LLJs are common during the entire year over almost all of the Arctic Ocean, with some seasonal and geographical variation.

All months show a distinct area of higher frequency of occurrence close to the sea-ice edge. LLJs in this area are likely forced by the horizontal temperature gradient, which is stronger in the colder months between ice and open sea. During the winter months, as the temperature gradient is very strong, the area of higher frequency of occurrence in the Barents Sea is very wide—it expands by more than 100 km,

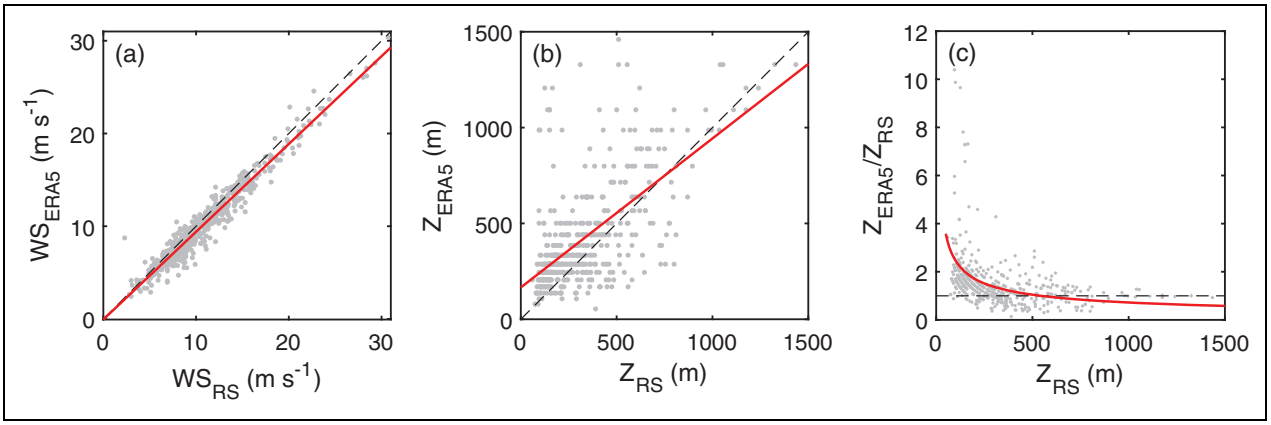


**Figure 8. Scatter plots comparing low-level jet (LLJ) speed and height for both data sets**. Comparison of LLJ properties from ERA5 and radiosondes (a) speed at jet peak, (b) jet height, and (c) the ratio of LLJ heights $Z_{ERA5}/Z_{RS}$. Black dashed lines show the 1:1 match between ERA5 and radiosondes; the red lines are those of best fit, being $y = 0.95x - 0.06$, $y = 0.78x + 165$, and $y = 29x^{-0.53}$, for (a), (b), and (c) respectively.

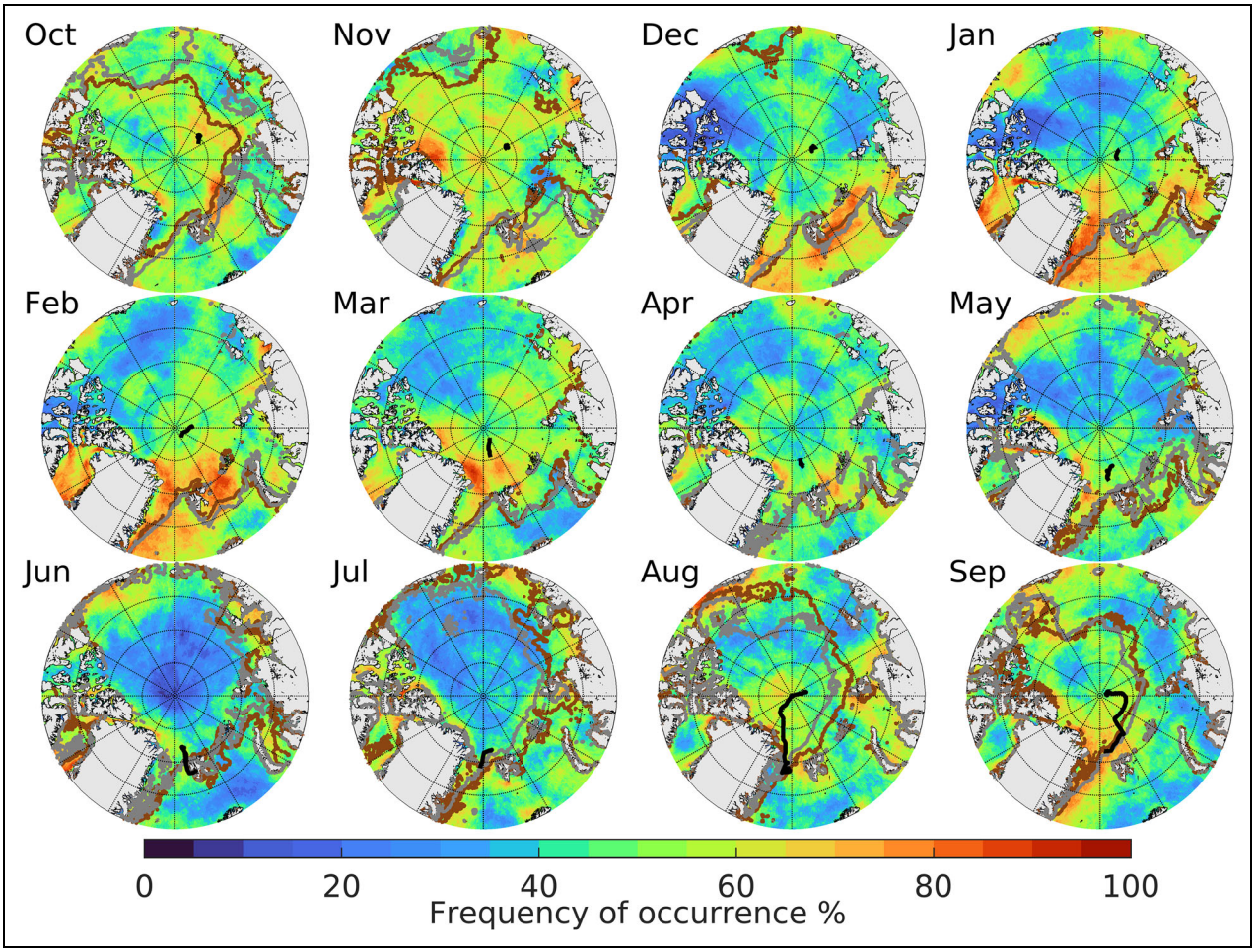


**Figure 9. Low-level jet frequency of occurrence for the Arctic Ocean**. Frequency of occurrence per month calculated by ERA5 reanalysis for the Multidisciplinary drifting Observatory for the Study of Arctic Climate year. Brown and gray lines indicate the sea-ice edge the first and last day of each month, respectively. The black line shows the ship's location over each month.

while in June and July, when the temperature gradient is at a minimum, this area of high occurrence is narrower.

On average, June and July have the lowest frequency, while the highest is from September to March. However, there are areas, especially between the Beaufort Sea and the East Siberian Sea from December onward, with low occurrence. These low-occurrence regions are far from the ice edge and thus lacking strong surface temperature

gradients which might force jets via either baroclinicity or inertial processes.

In order to more clearly show seasonal variability, we selected four points at which to examine LLJ frequency of occurrence, speed, and height. The four points are marked as circles in **Figure 1**; they are at the North Pole (NP); two fixed points, P1 and P2, at the same latitude, 85°, but opposite in longitude, P1 at −150° and P2 at 30°; and one moving point at the ice edge (IE), this has a fixed longitude of 45°, but a latitude changing to follow the sea-ice edge. The frequency of occurrence at each point is shown by month in **Figure 4**, along with those along the ship track from both radiosondes and ERA5. The individual points show more variability in jet occurrence than along the ship track, where seasonal and spatial effects are intertwined. All show some degree of seasonal cycle; notably all have a minimum in the summer, in June or July, and broad maxima during the winter. The frequency of occurrence around the IE is usually higher than at the rest of the points, with a minimum in June of 40%. The frequency of occurrence at the NP is at least 40% except in June and July, when it decreases below 30%. Although P1 and P2 have the same latitude, the variability in LLJ occurrence over time differs substantially between them; both have absolute maxima in late winter, April and March, respectively, but while P2 has a broad maximum throughout the winter, P1 has a broad minimum between January and March. During winter, P1 is much deeper into the sea ice than P2, and the number of forcing mechanisms for LLJs there is likely fewer. Text S2 and Figure S5 describe the seasonal probability distribution of LLJ height and speed for each point.

## 4. Conclusions

We have analyzed the frequency of occurrence and characteristics of LLJs for the full calendar year of the MOSAiC project, using observed wind profiles from radiosondes and model profiles from the ERA5 reanalysis. To our knowledge, this is the first time that LLJs have been characterized in the Arctic for all seasons. Our results show that LLJs are common throughout the entire year, with some seasonal differences in the frequency of occurrence, speed, and height.

The peak in observed jet height distributions was below 250 m throughout the year, lowest in winter and highest in summer. ERA5 has a consistent high bias in jet height, with a peak at or above 240 m, and seasonal variation in height opposite to that in the observations, being highest in winter and shallowest in summer, when it most closely matched the observed height distribution. In the mean, this bias is a function of observed jet height, with the bias being highest for the lowest jets, decreasing with jet altitude. For jets above about 1,000 m, the ERA5 jet heights closely match those observed.

The observed LLJs have a typical speed between 6 and 14 m $s^{-1}$, being fastest in winter and during the transition period between winter and the start of the summer melt. ERA5 represents the speed well, with only a small mean bias of –0.6 m $s^{-1}$ for the entire year, with the greatest bias in summer of about 0.8 m $s^{-1}$. This bias is a weak linear function of the observed jet speed.

Although a proper comparison with previous studies can be difficult since the objectives, time period, spatial focus, methods, and even the definition of an LLJ vary considerably, our results for LLJ height and speed agree well with the winter climatology of Tuononen et al. (2015). It has been assumed that LLJ activity is the greatest in the relatively colder months (Tuononen et al., 2015); however, here we find that, although they are more common in winter, LLJs are frequent during the entire year with an observed frequency of occurrence always higher than 40%. The ERA5 results show how the frequency depends on both the season and geographical location; they show the central Arctic Ocean had a frequency higher than 40% for all months except June and July, when it was less than 10% for some areas. The areas with the highest LLJ occurrence are close to the sea-ice edge during the entire year, but the spatial extent of this area varies strongly between seasons, being wider in winter and narrower in summer.

## Data accessibility statement

The radiosonde data used here are drawn from the Multidisciplinary drifting Observatory for the Study of the Arctic Climate archives at PANGAEA (https://www.pangaea.de/; Maturilli et al., 2021; http://dx.doi.org/10.1594/PANGAEA.928656). The ERA5 reanalysis data are available from the European Centre for Medium-Range Weather Forecasts at: https://www.ecmwf.int/en/forecasts/datasets/reanalysis-datasets/era5.

## Supplemental files

The supplemental files for this article can be found as follows:

Figures S1–S5. Docx
Text S1–S2. Docx

## Acknowledgments

Data used in this article were produced as part of the international Multidisciplinary drifting Observatory for the Study of the Arctic Climate (MOSAiC) with the tag MOSAiC20192020 and the Project_ID: AWI_PS122_00. We would like to thank everyone who contributed to the measurements used here (Nixdorf et al., 2021). Radiosonde data were obtained through a partnership between the leading Alfred Wegener Institute, the Atmospheric Radiation Measurement user facility, a U.S. Department of Energy facility managed by the Biological and Environmental Research Program, and the German Weather Service (DWD).

## Funding

The Multidisciplinary drifting Observatory for the Study of the Arctic Climate (MOSAiC) program was funded by the German Federal Ministry for Education and Research (BMBF) through financing the Alfred-Wegener-Institut Helmholtz Zentrum für Polarund Meeresforschung (AWI) and the Polarstern expedition PS122 under grant N-2014-H-060_Dethloff. IMB and RN were funded by the UK

Natural Environment Research Council (grant NE/S002472/1). VLG was funded by a scholarship from the Mexican Council of Science and Technology (CONACyT, studentship no. 2019-000026-01EXTF-00102). The radiosonde program was funded by AWI awards AFMOSAiC-1_00 and AWI_PS122_00, the U.S. Department of Energy Atmospheric Radiation Measurement Program, and the German Weather Service.

## Competing interests

The authors declare that they have no competing interests.

## Author contributions

Participated in the Multidisciplinary drifting Observatory for the Study of the Arctic Climate field campaign: IMB, SD.

Prepared the radiosonde data set: SD.

Designed the study: IMB, RN, VLG.

Conducted the data analysis and wrote the majority of the manuscript: VLG.

Contributed to this article: IMB, RN, SD.

## References

**Achtert, P**, **Brooks, IM**, **Brooks, BJ**, **Moat, BI**, **Prytherch, J**, **Persson, POG**, **Tjernström, M**. 2015. Measurement of wind profiles over the Arctic Ocean from ship-borne Doppler lidar. *Atmospheric Measurement Techniques* **8**: 4993–5007. DOI: http://dx.doi.org/10.5194/amt-8-4993-2015.

**Andreas, EL**, **Claffy, KJ**, **Makshtas, AP**. 2000. Low-level atmospheric jets and inversions over the western Weddell Sea. *Boundary-Layer Meteorology* **97**: 459–486. DOI: https://dx.doi.org/10.1023/A:1002793831076.

**Banta, R**, **Newsom, RK**, **Lundquist, JK**, **Pichugina, YL**, **Coulter, RL**, **Mahrt, L**. 2002. Nocturnal low-level jet characteristics over Kansas during cases-99. *Boundary-Layer Meteorology* **105**: 221–252. DOI: https://dx.doi.org/10.1023/A:1019992330866.

**Banta, RM**, **Pichugina, YL**, **Newsom, RK**. 2003. Relationship between low-level jet properties and turbulence kinetic energy in the nocturnal stable boundary layer. *Journal of the Atmospheric Sciences* **60**: 2549–2555. DOI: https://dx.doi.org/10.1175/1520-0469(2003)060<2549:RBLJPA>2.0.CO;2.

**Birch, CE**, **Brooks, IM**, **Tjernström, M**, **Shupe, M**, **Milton, SF**, **Earnshaw, P**, **Mauritsen, T**, **Sedlar, J**, **Persson, POG**, **Leck, C**. 2012. Modelling atmospheric structure, cloud and their response to CCN in the central Arctic: ASCOS case studies. *Atmospheric Chemistry and Physics* **12**: 3419–3435. DOI: https://dx.doi.org/10.5194/acp-12-3419-2012.

**Bonner, WD**. 1968. Climatology of the low level jet. *Monthly Weather Review* **96**: 833–850. DOI: https://dx.doi.org/10.1175/1520-0493(1968)096,0833:COTLLJ.2.0.CO;2.

**Bromwich, DH**, **Kuo, YH**, **Serreze, M**, **Walsh, J**, **Bai, LS**, **Barlage, M**, **Hines, K**, **Slater, A**. 2010. Arctic system reanalysis: Call for community involvement. *Eos Transactions* **91**: 13–14. DOI: https://dx.doi.org/10.1029/2010EO020001.

**Bromwich, DH**, **Wilson, AB**, **Bai, LS**, **Moore, GWK**, **Bauer, P**. 2015. A comparison of the regional Arctic System Reanalysis and the global ERA-Interim Reanalysis for the Arctic. *Quarterly Journal of the Royal Meteorological Society* **142**: 644–658. DOI: https://dx.doi.org/10.1002/qj.2527.

**Brooks, IM**, **Tjernström, M**, **Persson, POG**, **Shupe, MD**, **Atkinson, RA**, **Canut, G**, **Birch, CE**, **Mauritsen, T**, **Sedlar, J**, **Brooks, BJ**. 2017. The turbulent structure of the Arctic summer boundary layer during the Arctic Summer Cloud-Ocean Study. *Journal of Geophysical Research: Atmospheres* **122**: 9685–9704. DOI: https://doi.org/10.1002/2017JD027234.

**Conangla, L**, **Cuxart, J**. 2006. On the turbulence in the upper part of the low-level jet: An experimental and numerical study. *Boundary-Layer Meteorology* **118**: 379–400. DOI: https://doi.org/10.1007/s10546-005-0608-y.

**Graham, RM**, **Hudson, SR**, **Maturilli, M**. 2019. Improved performance of ERA5 in Arctic gateway relative to four global atmospheric reanalyses. *Geophysical Research Letters* **46**. DOI: https://dx.doi.org/10.1029/2019GL082781.

**Guest, P**, **Persson, POG**, **Wang, S**, **Jordan, M**, **Jin, Y**, **Blomquist, B**, **Fairall, C**. 2018. Low-level baroclinic jets over the new Arctic Ocean. *Journal of Geophysical Research: Oceans* **123**: 4074–4091. DOI: https://dx.doi.org/10.1002/2018JC013778.

**Hersbach, H**, **Bell, B**, **Berrisford, P**, **Hirahara, S**, **Horányi, A**, **Muñoz-Sabater, J**, **Simmons, A**. 2020. The ERA5 global reanalysis. *Quarterly Journal of the Royal Meteorological Society* **146**: 1999–2049. DOI: https://dx.doi.org/10.1002/qj.3803.

**Holland, MM**, **Bitz, CM**. 2003. Polar amplification of climate change in coupled models. *Climate Dynamics* **21**: 221–232. DOI: https://dx.doi.org/10.1007/s00382-003-0332-6.

**Jakobson, L**, **Vihma, T**, **Jakobson, E**, **Palo, T**, **Männik, A**, **Jaagus, J**. 2013. Low-level jet characteristics over the Arctic Ocean in spring and summer. *Atmospheric Chemistry and Physics* **13**: 11089–11099. DOI: https://dx.doi.org/10.5194/acp-13-11089-2013.

**Kalverla, PC**, **Duncan, JB**, **Jr., Steeneveld, GJ**, **Holtslag, AAM**. 2019. Low-level jets over the North Sea based on ERA5 and observations: Together they do better. *Wind Energy Science* **4**: 193–209. DOI: https://dx.doi.org/10.5194/wes-4-193-2019.

**Knust, R**. 2017. Polar research and supply vessel POLARSTERN operated by the Alfred-Wegener-Institute. *Journal of Large-scale Research Facilities* **3**: A119–A119. DOI: https://dx.doi.org/10.17815/jlsrf-3-163.

**Maturilli, M**, **Holdridge, DJ**, **Dahlke, S**, **Graeser, J**, **Sommerfeld, A**, **Jaiser, R**, **Deckelmann, H**, **Schulz, A**. 2021. *Initial radiosonde data from 2019-10 to 2020-09 during project MOSAiC*. Bremerhaven, Germany: Alfred Wegener Institute, Helmholtz Centre for

Polar and Marine Research. DOI: http://dx.doi.org/10.1594/PANGAEA.928656.

**Nicolaus, M**, **Perovich, DK**, **Spreen, G**, **Granskog, MA**, **Albedyll, LV**, **Angelopoulos, M**, **Anhaus, P**, **Arndt, S**, **Belter, HJ**, **Bessonov, V**, **Birnbaum, G**, **Brauchle, J**, **Calmer, R**, **Cardellach, E**, **Cheng, B**, **Clemens-Sewall, D**, **Dadic, R**, **Damm, E**, **de Boer, G**, **Demir, O**, **Dethloff, K**, **Divine, DV**, **Fong, AA**, **Fons, S**, **Frey, MM**, **Fuchs, N**, **Gabarró, C**, **Gerland, S**, **Goessling, HF**, **Gradinger, R**, **Haapala, J**, **Haas, C**, **Hamilton, J**, **Hannula, H-R**, **Hendricks, S**, **Herber, A**, **Heuzé, C**, **Hoppmann, M**, **Høyland, KV**, **Huntemann, M**, **Hutchings, JK**, **Hwang, B**, **Itkin, P**, **Jacobi, H-W**, **Jaggi, M**, **Jutila, A**, **Kaleschke, L**, **Katlein, C**, **Kolabutin, N**, **Krampe, D**, **Kristensen, SS**, **Krumpen, T**, **Kurtz, N**, **Lampert, A**, **Lange, BA**, **Lei, R**, **Light, B**, **Linhardt, F**, **Liston, GE**, **Loose, B**, **Macfarlane, AR**, **Mahmud, M**, **Matero, IO**, **Maus, S**, **Morgenstern, A**, **Naderpour, R**, **Nandan, V**, **Niubom, A**, **Oggier, M**, **Oppelt, N**, **Pätzold, F**, **Perron, C**, **Petrovsky, T**, **Pirazzini, R**, **Polashenski, C**, **Rabe, B**, **Raphael, IA**, **Regnery, J**, **Rex, M**, **Ricker, R**, **Riemann-Campe, K**, **Rinke, A**, **Rohde, J**, **Salganik, E**, **Scharien, RK**, **Schiller, M**, **Schneebeli, M**, **Semmling, M**, **Shimanchuk, E**, **Shupe, MD**, **Smith, MM**, **Smolyanitsky, V**, **Sokolov, V**, **Stanton, T**, **Stroeve, J**, **Thielke, L**, **Timofeeva, A**, **Tonboe, RT**, **Tavri, A**, **Tsamados, M**, **Wagner, DN**, **Watkins, D**, **Webster, M**, **Wendisch, M**. 2022. Overview of the MOSAiC expedition: Snow and sea ice. *Elementa: Science of the Anthropocene* **10**: 000046. DOI: https://dx.doi.org/10.1525/elementa.2021.000046.

**Nixdorf, U**, **Dethloff, K**, **Rex, M**, **Shupe, M**, **Sommerfeld, A**, **Perovich, DK**, **Nicolaus, M**, **Heuze, C**, **Rabe, B**, **Loose, B**, **Damm, E**, **Gradinger, R**, **Fong, A**, **Maslowski, W**, **Rinke, A**, **Kwok, R**, **Spreen, G**, **Wendisch, M**, **Herber, A**, **Hirsekorn, M**, **Mohaupt, V**, **Frickenhaus, S**, **Immerz, A**, **Weiss-Tuider, K**, **Koenig, B**, **Mengedoht, D**, **Regnery, J**, **Gerchow, P**, **Ransby, D**, **Krumpen, T**, **Morgenstern, A**, **Haas, C**, **Kanzow, T**, **Rack, F**, **Saitzev, V**, **Sokolov, V**, **Makarov, A**, **Schwarze, S**, **Wunderlick, T**, **Wurr, K**, **Boetius, A**. 2021. MOSAiC extended acknowledgement. *Zenodo*. DOI: http://dx.doi.org/10.5281/zenodo.5541624.

**Overland, J**, **Dunlea, E**, **Box, JE**, **Corell, R**, **Forsius, M**, **Kattsov, V**, **Olsen, MS**, **Pawlak, J**, **Reiersen, LO**, **Wang, M**. 2019. The urgency of arctic change. *Polar Science* **21**: 6–13. DOI: https://dx.doi.org/10.1016/j.polar.2018.11.008.

**Rabe, B**, **Heuzé, C**, **Regnery, J**, **Aksenov, Y**, **Allerholt, J**, **Athanase, M**, **Bai, Y**, **Basque, C**, **Bauch, D**, **Baumann, TM**, **Chen, D**, **Cole, ST**, **Craw, L**, **Davies, A**, **Damm, E**, **Dethloff, K**, **Divine, DV**, **Doglioni, F**, **Ebert, F**, **Fang, Y-C**, **Fer, I**, **Fong, AA**, **Gradinger, R**, **Granskog, MA**, **Graupner, R**, **Haas, C**, **He, H**, **He, Y**, **Hoppmann, M**, **Janout, M**, **Kadko, D**, **Kanzow, T**, **Karam, S**, **Kawaguchi, Y**, **Koenig, Z**, **Kong, B**, **Krishfield, RA**, **Krumpen, T**, **Kuhlmey, D**, **Kuznetsov, I**, **Lan, M**, **Laukert, G**, **Lei, R**, **Li, T**, **Torres-Valdés, S**, **Lin, L**, **Lin, L**, **Liu, H**, **Liu, N**, **Loose, B**, **Ma, X**, **MacKay, R**, **Mallet, M**, **Mallett, RDC**, **Maslowski, W**, **Mertens, C**, **Mohrholz, V**, **Muilwijk, M**, **Nicolaus, M**, **O'Brien, JK**, **Perovich, D**, **Ren, J**, **Rex, M**, **Ribeiro, N**, **Rinke, A**, **Schaffer, J**, **Schuffenhauer, I**, **Schulz, K**, **Shupe, MD**, **Shaw, W**, **Sokolov, V**, **Sommerfeld, A**, **Spreen, G**, **Stanton, T**, **Stephens, M**, **Su, J**, **Sukhikh, N**, **Sundfjord, A**, **Thomisch, K**, **Tippenhauer, S**, **Toole, JM**, **Vredenborg, M**, **Walter, M**, **Wang, H**, **Wang, L**, **Wang, Y**, **Wendisch, M**, **Zhao, J**, **Zhou, M**, **Zhu, J**. 2022. Overview of the MOSAiC expedition: Physical oceanography. *Elementa: Science of the Anthropocene* **10**(1): 00062. DOI: https://dx.doi.org/10.1525/elementa.2021.00062.

**Ranjha, R**, **Svensson, G**, **Tjernström, M**, **Semedo, A**. 2013. Global distribution and seasonal variability of coastal low-level jets derived from ERA-Interim reanalysis. *Tellus A: Dynamic Meteorology and Oceanography* **65**: 20412. DOI: http://dx.doi.org/10.3402/tellusa.v65i0.20412.

**Serreze, MC**, **Barrett, AP**, **Stroeve, JC**, **Kindig, DN**, **Holland, MM**. 2009. The emergence of surface-based Arctic amplification. *The Cryosphere* **3**: 11–19. DOI: https://dx.doi.org/10.5194/tc-3-11-2009.

**Shupe, MD**, **Persson, POG**, **Brooks, IM**, **Tjernström, M**, **Sedlar, J**, **Mauritsen, T**, **Leck, C**, **Sjogren, S**. 2013. Cloud and boundary layer interactions over the Arctic sea-ice in late summer. *Atmospheric Chemistry and Physics* **13**: 9379–9400. DOI: http://dx.doi.org/10.5194/acp-13-9379-2013.

**Shupe, MD**, **Rex, M**, **Blomquist, B**, **Persson, POG**, **Schmale, J**, **Uttal, T**, **Althausen, D**, **Angot, H**, **Archer, S**, **Bariteau, L**, **Beck, I**, **Bilberry, J**, **Bucci, S**, **Buck, C**, **Boyer, M**, **Brasseur, Z**, **Brooks, IM**, **Calmer, R**, **Cassano, J**, **Castro, V**, **Chu, D**, **Costa, D**, **Cox, CJ**, **Creamean, J**, **Crewell, S**, **Dahlke, S**, **Damm, E**, **de Boer, G**, **Deckelmann, H**, **Dethloff, K**, **Dütsch, M**, **Ebell, K**, **Ehrlich, A**, **Ellis, J**, **Engelmann, R**, **Fong, AA**, **Frey, MM**, **Gallagher, MR**, **Ganzeveld, L**, **Gradinger, R**, **Graeser, J**, **Greenamyer, V**, **Griesche, H**, **Griffiths, S**, **Hamilton, J**, **Heinemann, G**, **Helmig, D**, **Herber, A**, **Heuzé, C**, **Hofer, J**, **Houchens, T**, **Howard, D**, **Inoue, J**, **Jacobi, H-W**, **Jaiser, R**, **Jokinen, T**, **Jourdan, O**, **Jozef, G**, **King, W**, **Kirchgaessner, A**, **Klingebiel, M**, **Krassovski, M**, **Krumpen, T**, **Lampert, A**, **Landing, W**, **Laurila, T**, **Lawrence, D**, **Lonardi, M**, **Loose, B**, **Lüpkes, C**, **Maahn, M**, **Macke, A**, **Maslowski, W**, **Marsay, C**, **Maturilli, M**, **Mech, M**, **Morris, S**, **Moser, M**, **Nicolaus, M**, **Ortega, P**, **Osborn, J**, **Pätzold, F**, **Perovich, DK**, **Petäjä, T**, **Pilz, C**, **Pirazzini, R**, **Posman, K**, **Powers, H**, **Pratt, KA**, **Preußer, A**, **Quéléver, L**, **Radenz, M**, **Rabe, B**, **Rinke, A**, **Sachs, T**, **Schulz, A**, **Siebert, H**, **Silva, T**, **Solomon, A**, **Sommerfeld, A**, **Spreen, G**, **Stephens, M**, **Stohl, A**, **Svensson, G**, **Uin, J**, **Viegas, J**, **Voigt, C**, **von der Gathen, P**, **Wehner, B**, **Welker, JM**, **Wendisch, M**, **Werner, M**, **Xie, ZQ**, **Yue, F**. 2022. Overview of the MOSAiC expedition—

Atmosphere. *Elementa: Science of the Anthropocene* **10**(1): 00060. DOI: https://dx.doi.org/10.1525/elementa.2021.00060.

**Sotiropoulou, G**, **Sedlar, J**, **Forbes, R**, **Tjernström, M**. 2016. Summer Arctic clouds in the ECMWF forecast model: An evaluation of cloud parameterization schemes. *Quarterly Journal of the Royal Meteorological Society* **142**: 387–400. DOI: https://dx.doi.org/10.1002/qj.2658.

**Tjernström, M**, **Leck, C**, **Persson, POG**, **Jensen, ML**, **Oncley, SP**, **Targino, A**. 2004. The summertime Arctic atmosphere: Meteorological measurements during the Arctic Ocean Experiment 2001. *Bulletin of the American Meteorological Society* **85**(9): 1305–1322. DOI: http://dx.doi.org/10.1175/BAMS-85-9-1305.

**Tjernström, M**, **Shupe, MD**, **Brooks, IM**, **Achtert, P**, **Prytherch, J**, **Sedlar, J**. 2019. Arctic summer airmass transformation, surface inversions and the surface energy budget. *Journal of Climate* **32**: 769–789. DOI: http://dx.doi.org/10.1175/JCLI-D-18-0216.1.

**Tjernström, M**, **Shupe, MD**, **Brooks, IM**, **Persson, POG**, **Prytherch, J**, **Salisbury, DJ**, **Sedlar, J**, **Achtert, P**, **Brooks, BJ**, **Johnston, PE**, **Sotiropoulou, G**, **Wolfe, D**. 2015. Warm-air advection, air mass transformation and fog causes rapid ice melt. *Geophysical Research Letters* **42**: 5594–5602. DOI: http://dx.doi.org/10.1002/2015GL064373.

**Tjernström, M**, **Svensson, G**, **Magnusson, L**, **Brooks, IM**, **Prytherch, J**, **Vüllers, J**, **Young, G**. 2021. Central arctic weather forecasting: Confronting the ECMWF IFS with observations from the Arctic Ocean 2018 expedition. *Quarterly Journal of the Royal Meteorological Society* **147**: 1278–1299. DOI: http://dx.doi.org/10.1002/qj.3971.

**Tuononen, M**, **Sinclair, V**, **Vihma, T**. 2015. A climatology of low-level jets in the mid-latitudes and polar regions of the Northern Hemisphere. *Atmospheric Science Letters* **16**(4): 492–499. DOI: http://dx.doi.org/10.1002/asl.587.

**Young, G**, **Vüllers, J**, **Achtert, P**, **Field, P**, **Day, JJ**, **Forbes, R**, **Price, R**, **O'Connor, E**, **Tjernström, M**, **Prytherch, J**, **Neely III, R**, **Brooks, IM**. 2021. Evaluating Arctic clouds modelled with the Unified Model and Integrated Forecasting System. *Atmospheric Chemistry and Physics Discussions*. DOI: https://dx.doi.org/10.5194/acp-2021-662.



**How to cite this article:** López-García, V, Neely III, RR, Dahlke, S, Brooks, IM. 2022. Low-level jets over the Arctic Ocean during MOSAiC. *Elementa: Science of the Anthropocene* 10(1). DOI: https://doi.org/10.1525/elementa.2022.00063

**Domain Editor-in-Chief:** Detlev Helmig, Boulder AIR LLC, Boulder, CO, USA

**Knowledge Domain:** Atmospheric Science

**Part of an Elementa Special Feature:** The Multidisciplinary Drifting Observatory for the Study of Arctic Climate (MOSAiC)

**Published:** September 14, 2022 **Accepted:** August 7, 2022 **Submitted:** May 7, 2022



ELEMENTA Science of the Anthropocene

*Elem Sci Anth* is a peer-reviewed open access journal published by University of California Press.

OPEN ACCESS